Article:
Seo, K, Lee, J orcid.org/0000-0002-7768-7061, Jo, J et al. (2 more authors) (2019) Highly Efficient (>10%) Flexible Organic Solar Cells on PEDOT-Free and ITO-Free Transparent Electrodes. Advanced Materials, 31 (36). 1902447. ISSN 0935-9648

https://doi.org/10.1002/adma.201902447

Highly efficient (>10%) flexible organic solar cells on PEDOT-free and ITO-free transparent electrodes

Ki-Won Seo[1], Jaemin Lee[2], Jiwhan Jo[1], Changsoon Cho[1], and Jung-Yong Lee[1,3,*]

[1]School of Electrical Engineering (EE), Korea Advanced Institute of Science and Technology (KAIST), Daejeon 34141, Republic of Korea

[2]Department of Chemistry, University of Warwick, Coventry, CV4 7AL, United Kingdom

[3]Graduate School of Energy, Environment, Water, and Sustainability (EEWS), Korea Advanced Institute of Science and Technology (KAIST), Daejeon 34141, Republic of Korea

[*]All correspondence should be addressed to J.-Y.L. (email: jungyong.lee@kaist.ac.kr)

Keywords: PEDOT-free, ITO-free, AgNN, transparent electrodes, flexible organic solar cells

Abstract

We present a novel approach to fabricate flexible organic solar cells without indium tin oxide (ITO) and poly(3,4-ethylenedioxythiophene)-poly(styrenesulfonate) (PEDOT:PSS). We use junction-free metal nanonetworks (NNs) as transparent electrodes. The metal NNs are monolithically etched using nanoscale shadow masks, and they exhibit excellent optoelectronic performance. Furthermore, the optoelectrical properties of the NNs can be controlled by both the initial metal layer thickness and NN density. Hence, with an extremely thin silver layer, the appropriate density control of the networks can lead to high transmittance and low sheet resistance. Such NNs can be utilized for thin film devices without planarization by conductive materials such as PEDOT:PSS. As a result, we successfully fabricate a highly efficient flexible organic solar cell with a power conversion efficiency (PCE) of 10.6% and high device yield (93.8%) on PEDOT-free and ITO-free transparent electrodes. Furthermore, the flexible solar cell retains 94.3% of the initial PCE even after 3000 bending stress tests (strain: 3.13%).

Introduction

As the demand for wearable devices has increased, lightweight organic solar cells (OSCs)[1, 2] have attracted attention as a power source for such devices. Furthermore, recent advances in material development have led to increase in the efficiency of OSCs. This has enhanced the possibility of the application of OSCs to wearable devices.[3-9]

Conventional indium tin oxide (ITO), which is commonly used as an electrode in thin film optoelectronic devices, may not be suitable for flexible OSCs (FOSCs) owing to its brittle nature. Promising ITO alternatives, such as carbon nanotubes, conducting polymers, and graphene and metallic nanowires (NWs), have been proposed for flexible applications.[10-17] AgNWs are considered as the most promising TCEs for FOSCs based on their mechanical stability and superior optoelectrical characteristics.[13, 18, 19] However, the nonuniform and uncontrollable morphology of randomly stacked NW networks can frequently cause short circuiting unless they are flattened or covered by thick buffer layers. Moreover, the high junction resistance between NWs limits the conductivity of the entire film.[20, 21] Junctions radiate locally concentrated heat under current flow, which can cause electrodes and devices to fail. The weak adhesion of AgNW networks to substrates might have an adverse impact on the mechanical reliability of the devices fabricated using the substrates.[22, 23] These drawbacks currently limit the applicability of metal NW networks in optoelectronic devices.

A few studies have utilized electrospun polymer fibers networks to fabricate junction-free metal networks, thus overcoming the drawbacks of metal NWs.[24-26] Polymer fibers can be used as seed material for the electroless deposition of metals or as a shadow mask for etching underlying metal films. The latter is a top-down fabrication process proposed by Azuma *et al.*, and it is particularly beneficial for thin film optoelectronic devices.[27] Based on the top-down etching technique, zero-junction Cu, Al, and Au networks have been successfully fabricated for various applications such as touch screens, organic light-emitting diodes, and photodetectors. In previous works, metal networks can be used for photodetectors with an active layer thickness of over 250 nm.[28] An additional poly(3,4-ethylenedioxythiophene)-poly(styrenesulfonate) (PEDOT:PSS) layer was essential for

achieving high performance OLED devices. However, the acidity of PEDOT:PSS could adversely affect the subsequent organic layers on an electrode, which might limit its application to various devices.[29-32] Choi *et al.* pointed out that a network height of 80 nm was extremely *rough* for a 140-nm-thick OLED active layer.[33] Thus, there are few reports on high efficiency thin film FOSCs (> 10%) that use this type of metal networks.

Herein, we report highly efficient organic photovoltaic cells on flexible substrates without PEDOT:PSS and ITO. We used transparent conductive electrodes based on a conductive AgNN. The electrodes were fabricated by dry etching pre-deposited thin metal films using randomly distributed nanofiber networks, which acted as shadow masks. This process is highly compatible with various metal electrodes and substrates such as polyethylene phthalate (PET), polyimide (PI), polydimethylsiloxane (PDMS), and polyethylene naphthalate (PEN). More importantly, even with an initial Ag layer as thin as 15 nm, density control can achieve high optical transmittance with low sheet resistance. Consequently, we successfully fabricated highly efficient FOSCs with a power conversion efficiency (PCE) of 10.6%. The FOSCs were mechanically robust and retained 94.3% of the initial PCE even after 3000 bending tests (strain: 3.13%).

Results

Formation of etched conductive networks

Ag thin films were prepared on various target substrates through thermal evaporation to form etched AgNNs, as shown in Figure 1a(I). Then, electrospun polymer (we used poly (methyl methacrylate) (PMMA)) nanofibers were coated on the films using an electrospinning system (Fig. 1a(II)). The nanofibers were used as nanostructured shadow masks (hereafter referred to as nanomasks) during the subsequent dry etching process. Then, a nanomask-metal film composite was etched by employing an ion beam etching system, which is an anisotropic etching method (Fig. 1a(III)). Finally, after the etching process, flat etched NNs were formed underneath the nanomasks (Fig. 1a(IV)). The experimental details are described in the Method part. Figure 1b shows the scanning electron microscope (SEM) image of the electrospun polymer nanofibers. Mesh-like nanomasks were formed on the conductive films. Upon etching, the monolithic NNs were replicated on the substrates, as shown in Figure 1c and the inset. Note that the cross section of the NNs has a trapezoidal shape (see the inset of Fig. 1c). In addition, the contact resistance of the etched NNs is intrinsically zero, as shown in Figure 1c, in contrast to conventional AgNW random networks.[20-22] Consequently, it is not required to subject the etched NNs to any of the post-fabrication processes mentioned above. We also coated AgNWs on the same substrate using a spray coating method to compare surface morphology, roughness, electrical and optical properties, and chemical and thermal stability.

Atomic force microscopy characterization revealed that the surface roughness of the fabricated NNs was significantly lower than that of conventional AgNW networks, as shown in Figure 1d and e. The etched NNs exhibited uniform height and a 34% lower root mean square surface roughness (R_{rms}) compared to AgNWs, as shown in Supplementary Figure 1. Note that the final maximum height of the NNs is limited only by the initial thickness of the as-deposited metal films.

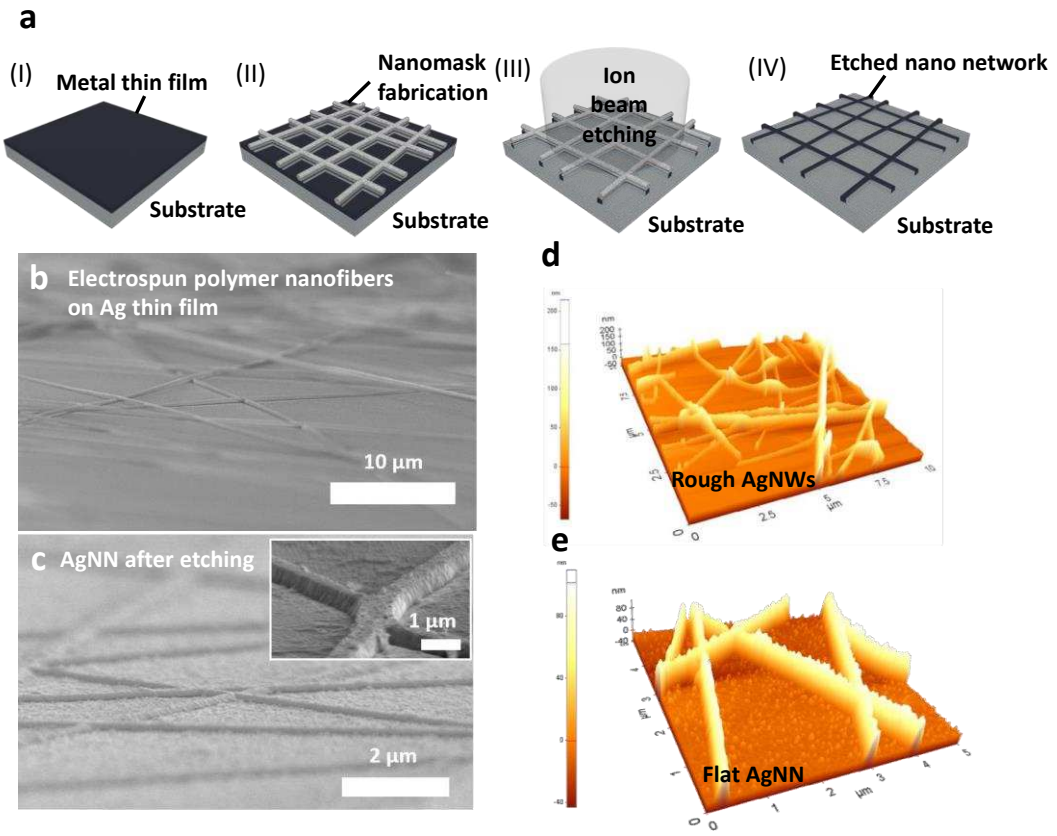

Fig 1. K.-W Seo et al.

Optoelectrical performances: AgNWs, AgNN electrode

To investigate the optoelectrical characteristics of the etched monolithic NNs, we measured the transmittances and sheet resistances of the electrodes and compared them with those of other TCEs. We compared optoelectrical properties in terms of the ratio of direct current conductivity (σ_{DC}) to optical conductivity (σ_{Op}), which is typically used as a figure of merit (FoM) of films.[34, 35] Conventional ITO films and AgNW films typically exhibit a σ_{DC}/σ_{Op} value of 400–800 and approximately 500 or lower, respectively.[35] The etched NNs showed a high transmittance of up to 94.4% at a sheet resistance of 2.4 Ω/sq, as shown in Figure 2a. This transmittance is higher than those of other ITO alternatives for similar sheet resistances, resulting in an FoM of approximately 3000. The FoM values of 300-nm-thick and 100-nm-thick AgNNs were approximately 3000 and 1000, respectively. To the best of our knowledge, an FoM of 3000 is among the highest obtained for alternatives to ITO.[35, 36]

The optoelectrical characteristics of our AgNN electrode can be controlled by both the initial Ag thickness and PMMA fiber density, whereas those of conventional AgNW networks can be controlled only by the density of NWs. Figure 2b shows the sheet resistance and transmittance of the AgNN with respect to Ag thickness and the AgNN coverage ratio. For example, reasonably low sheet resistance (< 15 Ω/sq) and high transmittance (90%) were obtained in a 50-nm-thick Ag film with a coverage of 19% (FoM: 324) and in a 25-nm-thick Ag film with a coverage of 36% (FoM: 248) (see arrows in Fig. 2b).

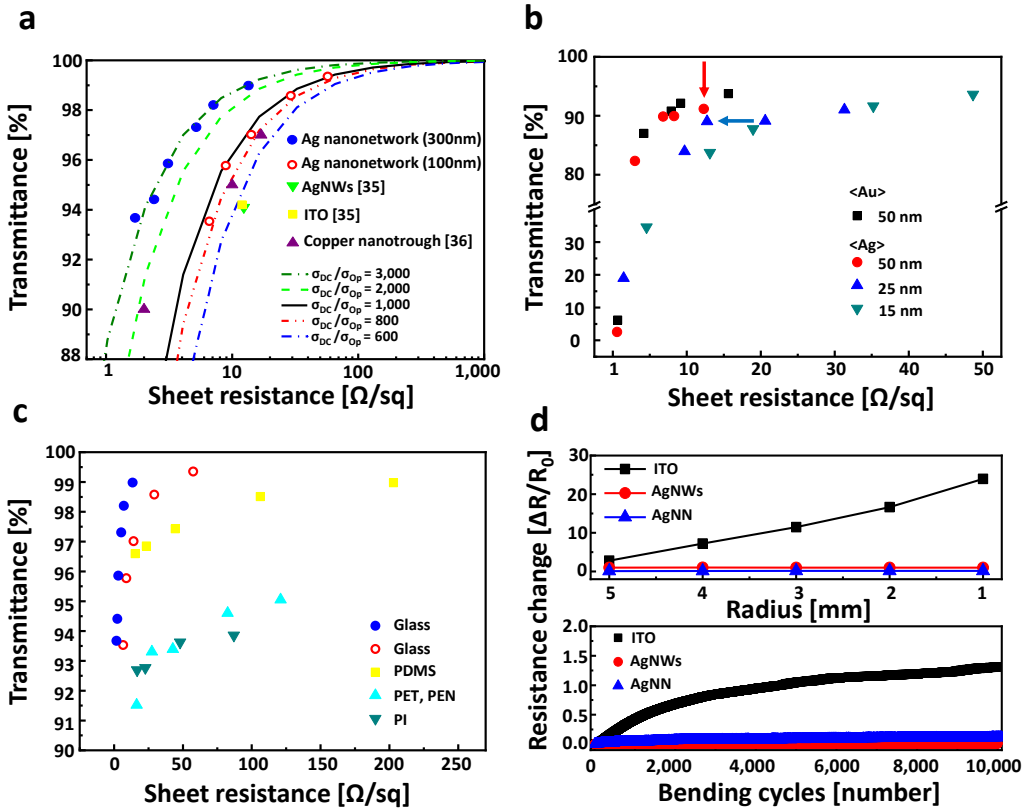

Fig 2. K.-W Seo et al.

Furthermore, various metal NN structures on various substrates can be fabricated as described above (Fig. 2b and 2c). We fabricated an Au NN (thickness: 50 nm) electrode using the same fabrication process. The Au NN electrode showed a sheet resistance of 4.21 to 15.6 Ω/sq and a transmittance of 87.1 to 93.7% with varying NN density (Fig. 2b). Figure 2c and Supplementary Figure 2 show the optoelectrical characteristics of the etched Ag networks formed on various

substrates. The characteristics were comparable to those of conventional TCEs.[22] These results indicate that the etched metal network electrode can be formed on almost any type of substrate regardless of surface conditions. More details are provided in Supplementary Information.

To investigate the mechanical robustness of the AgNN, we measured the change in resistance while reducing bending radius (Fig. 2d top) and during 10,000 bending cycling tests (Fig. 2d bottom). As shown in Figure 2d, the resistance of the etched AgNN electrode and AgNWs remained unchanged down to a bending radius of 1 mm. However, the ITO electrode, which is a well-known brittle material,[23, 37] showed a 25-fold increase in resistance at a bending radius of 1mm. During the cycling test, the resistance of the ITO electrode increased steadily while those of the AgNWs and AgNN electrode were almost unchanged.

The high performance of the etched NN can be attributed to the following factors. First, the etched NN is fabricated from bulk Ag, whose conductivity is approximately eight times higher than that of AgNWs. This high conductivity ensures that the overall sheet resistance of the etched NN electrodes is lower than that of ordinary metal NW electrodes. Next, the absence of junction resistance results in the overall transmittance being high even at sheet resistances lower than 10 Ω/sq because sheet resistance sensitively depends on junction resistance.[20, 21, 38] For AgNW networks, the addition of NWs in the low-sheet-resistance region rapidly decreases transmittance instead of improving the conductivity of the entire electrode owing to high contact resistance. The proportional relationship between contact resistance and sheet resistance is clearly observed. The decrease in contact resistance is a critical factor that determines the low sheet resistance of the entire network (Supplementary Fig. 3a-c). Additionally, the junction-free structure enhances thermal and chemical stability (Supplementary Fig. 3d-f).

Flexible organic solar cell device performances

Compared to devices on ITO electrodes, devices on nonplanar transparent electrodes, such as AgNWs, tend to show lower performance or device yield because of the nonuniform thickness of

active layers. Therefore, previous studies attempted to reduce surface roughness by hybridizing them with other conductive materials.[14, 33, 39-41] However, surface planarization with thin layers may not be effective if the step heights of electrodes are considerably higher than the thickness of the subsequent layer. Herein, we aimed to develop electrodes with the smallest step height while retaining the desired high transmittance and low sheet resistance. We selected a thickness of 15 nm for the electrodes, which showed a transmittance of 91.6% and a sheet resistance of 35.2 Ω/sq.

We fabricated FOSCs using fullerene-based phenyl-C70-butyric acid methyl ester ($PC_{70}BM$)[6-9] and a recently emerging non-fullerene-based acceptor, (2,2′-((2Z,2′Z)-(((4,4,9,9-tetrakis(4-hexylphenyl)-4,9-dihydro-s-indaceno[1,2-b:5,6-b′]dithiophene-2,7-diyl)bis(4-((2-ethylhexyl)oxy)thiophene-5,2-diyl)) bis(methanylylidene))bis(5,6-difluoro-3-oxo-2,3-dihydro-1H-indene-2,1-diylidene))dimalononitrile (IEICO-4F)[3-5](Fig. 3a and Supplementary Fig. 4), on the AgNN electrodes. The device structure was PET (125 μm)/ITO [or PEN (125 μm)/AgNN]/ZnO (40 nm)/PTB7-Th:$PC_{70}BM$ (100 nm) or IEICO-4F (150 nm)/MoO_3 (10 nm)/Ag (150 nm). Note that 0.6 wt% Zonyl was added to ZnO to enhance wettability.[34, 42] The photovoltaic performance and current density–voltage (*J-V*) characteristics of the FOSCs are summarized in Table 1 and Figure 3b. The devices fabricated on ITO and the AgNN exhibited PCEs of 8.35% and 8.31% (PTB7-Th:$PC_{70}BM$), respectively, and 9.59% and 10.6% (PTB7-Th:IEICO-4F), respectively. In particular, as shown in Figure 3c, our AgNN-based FOSCs (PTB7-Th:IEICO-4F) showed higher external quantum efficiency (EQE) compared to ITO-based FOSCs because the transmittance of the AgNN electrode was higher (Supplementary Fig. 5d). As a result, the short circuit current density (J_{sc}) and PCE of the AgNN-based FOSC were higher than those of the ITO-based FOSC.

Next, we investigated the effect of the step height of AgNN electrodes on FOSC performance. We prepared Ag films with thicknesses of 100, 70, 50, and 15 nm. We fabricated the FOSCs using AgNN electrodes and coated Zonyl added ZnO layer for inverted FOSCs. We learned that Zonyl FS-300 improves the wettability of the ZnO layer on the flexible substrate without surface treatment. It was found that 0.6 wt% Zonyl maximized the uniformity of ZnO and consequently maximized the device

yield and PCE (Supplementary Fig. 6).

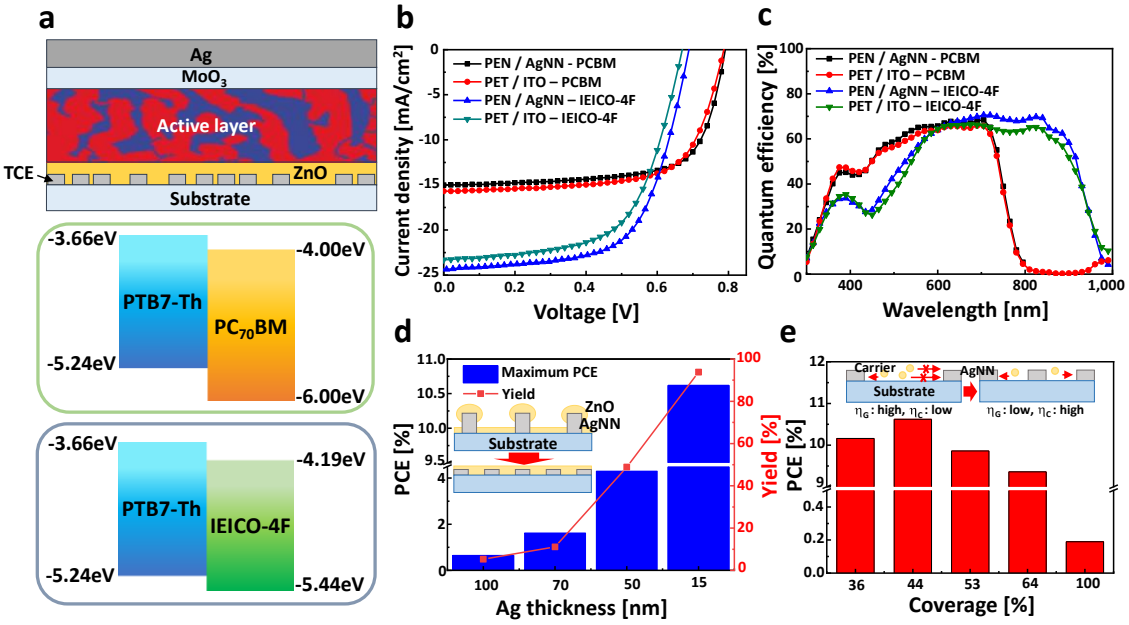

Fig 3. K.-W Seo et al.

Despite the improved wettability of ZnO, it could not cover the 100-nm-thick AgNN electrode smoothly owing to the large step height. Hence, a low yield of 5.3% and a maximum PCE of 0.65% were obtained (Fig. 3d and Supplementary Fig. 7). As the Ag layer became thinner, the ZnO layer (40 nm) covered the empty spaces of the NN structures more completely, increasing the PCE and yield of FOSCs (see inset of Fig. 3d). The 15-nm-thick AgNN-based FOSC showed the highest yield of 93.8%. The active layer covered the ZnO layer evenly, resulting in the highest PCE of 10.6%.

In fact, any transport layer can replace ZnO on the AgNN as long as it can cover AgNN completely. We applied PEDOT:PSS as shown in Supplementary Figure 8a. The FOSCs that used PEDOT:PSS as a transport layer on the 15-nm-thick AgNN electrode exhibited a PCE of 6.32%. However, the sheet resistance of AgNN increased from 19.3 to 30.7 Ω/sq after 9 days because of oxidization. This caused the degradation of device performance with time (4.43% PCE) because of the acidity of PEDOT:PSS

(Supplementary Fig. 8b). More details are provided in Supplementary Information.

Figure 3e shows the variation in PCE caused by the coverage of the 15-nm-thick AgNN. Supplementary Figure 9 shows the SEM images of the electrodes. The maximum PCE was 10.6% at a coverage of 44%, and the PCE was 0.19% at a coverage of 100% because of a low transmittance of 34.5% (Supplementary Fig. 5c). Interestingly, the PCE was 10.1% at a coverage of 36% even with higher transmittance. Generally, the empty spaces between networks should be minimized to reduce loss in charge collection because the carrier diffusion lengths in organic materials tend to be short. However, the amount of light transmitted through the electrodes decreases if network coverage becomes extremely large (see inset of Fig. 3e). Therefore, charge generation and collection should be considered for the high efficiency of FOSCs.

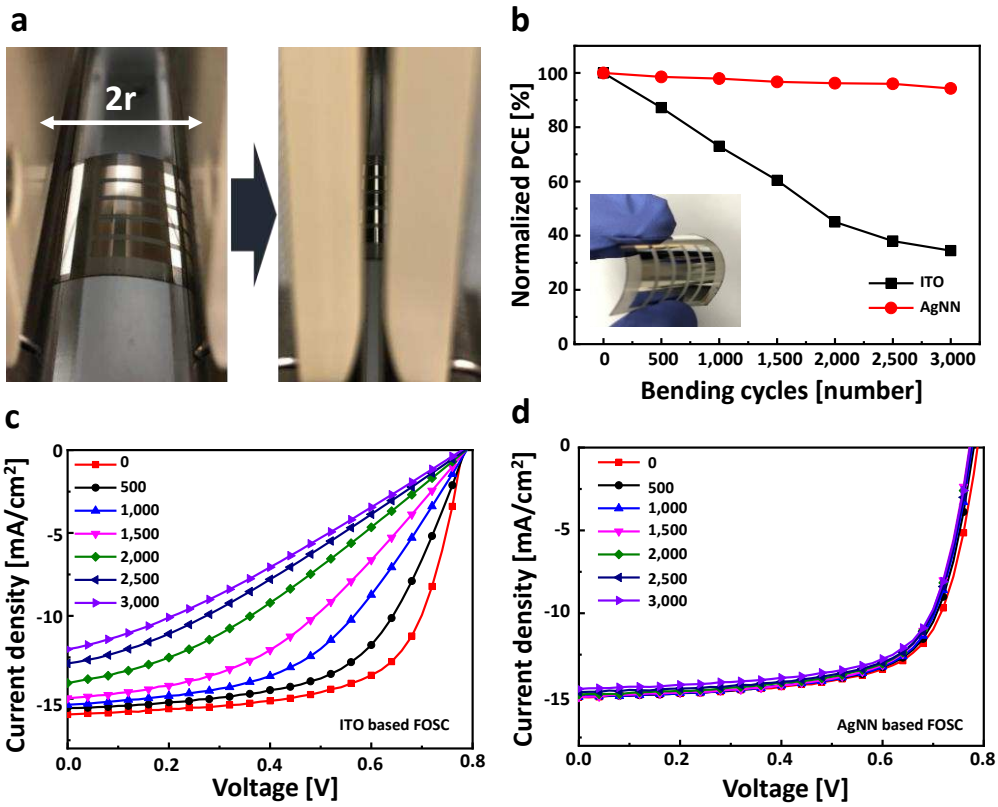

Fig 4. K.-W Seo et al.

Furthermore, the mechanical stability of devices is critical in FOSCs. We measured the PCEs of the PTB7-Th:$PC_{70}BM$-based FOSC devices during 3000 bending cycling tests as shown Figure 4a

(bending strain: 3.13%, 1.5 Hz, substrate thickness: 125 μm). We scanned the device every 500 times during the tests. As shown in Figure 4b, the PCE of the ITO-based FOSC was 34.5% of the initial PCE (8.21%) after the 3000 tests. Short circuit current density (J_{sc}) decreased from 15.95 to 12.01 mA/cm^2, and the fill factor (*FF*) decreased from 0.66 to 0.30 (Fig. 4c). In contrast, the AgNN-based FOSC showed almost constant *J-V* characteristics and retained 94.3% of the initial PCE even after 3000 bending cycles (Fig. 4d).

Steady efficiency under the repeated mechanical deformation of the AgNN-based FOSC suggests that the monolithic NN electrode etched without using PEDOT:PSS can be an ideal alternative to ITO as a transparent electrode for high performance flexible optoelectronic devices.

Conclusions

In this study, we investigated the fabrication and characteristics of junction-resistance-free metallic networks with smooth surface morphology on various flexible substrates. The monolithic NNs showed transmittances of up to 94.4% and sheet resistances as low as 2.4 Ω/sq with high thermal, environmental, and mechanical stabilities. Moreover, the height and morphological roughness of the networks could be controlled by changing the initial metal thickness and NN coverage. Coverage control with a small step height (15 nm) enabled us to achieve a high PCE of 10.6% using only a ZnO ETL layer without any other conductive materials. Furthermore, constant PCE of the AgNN-based-FOSC after 3000 bending cycles suggested that the AgNN electrode is perfectly suitable for flexible thin film devices with excellent mechanical stability.

Methods

Materials: PMMA, N,N-dimethylformamide, zinc acetate dehydrate, ethanolamine, were purchased from Sigma Aldrich Co., Ltd. The PET/ITO films were purchased from Toray, Japan. PTB7-Th, $PC_{70}BM$, IEICO-4F were purchased from 1-material, Canada. Zonyl FS-300 was purchased from Thermo Fisher Scientific Chemicals Co., Ltd. The PEDOT:PSS aqueous solutions of Clevios AI4083 was purchased from Heraeus, Germany.

AgNW synthesis: The AgNW solutions were prepared using a modified polyol process.[43-45] The final products were washed using glass filters. The washed AgNWs were stored in methanol.[22]

Preparation of nanofibers: The polymer nanofibers were prepared by electrospinning PMMA. 0.36g of PMMA powder was dissolved into 6ml of N,N-dimethylformamide and acetone mixed solution (2:1 volume ratio). To dissolve the PMMA powder, the mixed solution was stirred during 12h at room temperature. The gauge of the syringe tip, voltage, distance between the electrodes, and flow rate of the polymer solution were 23 G, 9.8 kV, 16 cm, and 0.6 ml/h, respectively. The conditions were adjusted to vary the diameter of the nanofibers. The nanofibers were dried completely after electrospinning to remove the solvent present in the fibers.

Ag etching and fabrication of AgNN: The thermally deposited Ag thin films were etched using an Ar ion beam etching system. The etch rate was set to be 17.6 nm/min and the etching area was 1 $inch^2$. It should be noted that the Ag etch rate can be further increased over 300 nm/min and up to 1000 nm/min with additive gases such as oxygen and chlorine.[46, 47] The ion milling system (VSI, Korea) was used and the etching conditions for RF power, gas flow rate, gas pressure, beam current, and accelerator current are as follows: 50 W, 7 sccm, 5 x 10^{-4} Torr, 6 mA, and 2 mA, respectively. For a uniform etching, the RF power and flow rate should be carefully adjusted to avoid the under-cut etching. After the etching process, the etched AgNN was sonicated in acetone for 30 s to remove any residue left on the substrate and the network.

FDTD simulation: The simulation domain was assumed to be air and the AgNN structures were

analyzed with 5 nm meshes using a periodic boundary condition. The refractive index of Ag was obtained from the Palik's book. The simulation results for TE and TM modes were averaged to calculate Mie efficiencies and estimate transmittance and haze of AgNNs as described in Supplementary Information.

Sheet resistance calculation: Sheet resistance was calculated from the equivalent circuit of a given random mesh of AgNW (length: 15 μm, diameter: 60 nm) and AgNN. The resistivity (ρ) of Ag was assumed to be 1.59×10^{-8} Ω·m. Since the calculation is based on the randomly generated structures, the average values were chosen from the sufficient number (5 ~ 300) of repeated simulations.

ZnO sol-gel synthesis: 1g of zinc acetate dehydrate is dissolved into 2-methoxyethanol 10ml in a vial with 0.28g of ethanolamine as a stabilizer and 0.6 wt% of Zonyl-FS 300 fluoro surfactant.[48] The mixed solution was stirred during 12h and aged 1 day at room temperature.

Device fabrication: ZnO layer was spun with 3000rpm, 30s on PET/ITO and PEN/AgNN and annealed at 140˚C (PET/ITO) and 160˚C (PEN/AgNN) for 30min in air. After the substrates were transferred into a nitrogen-filled glove box, PTB7-Th: $PC_{70}BM$ (25mg/ml, 1:1.5 weight ratio, chlorobenzene:1,8-didoctane (DIO) = 97:3, v/v) and PTB7-Th:IEICO-4F (20mg/ml, 1:1.5 weight ratio, chlorobenzene:chloronaphthalene = 96:4, v/v) layers were spun. Finally, MoO_3 (10 nm) and Ag (150 nm) were thermally evaporated on top of the active layers through a shadow mask under vacuum $<10^{-7}$Torr. The active area of the fabricated devices was ~0.15cm^2

Device Characterizations: Current density-voltage (*J-V*) characteristics were measured under irradiance of 100 mW/cm^2 utilizing a solar simulator (K201 LAB55, McScience). The external quantum efficiency (EQE) was acquired using a spectral measurement system (K3100 IQX, McScience Inc.).

Measurement and analysis: The total transmittances of the various samples were measured with an ultraviolet-visible (UV-vis) spectrophotometer (UV-3600, Shimadzu, Japan). The specular transmittances were also measured using a UV-vis spectrophotometer (UV-3100, Sinco, Korea). The

sheet resistances were measured using a four-point probe (Dasol Eng., Korea). The morphologies and current flows of the AgNWs, as well as those of the NN, were measured simultaneously using an XE-100 system (Park System, Korea).

References

1. Kaltenbrunner, M. et al. Ultrathin and lightweight organic solar cells with high flexibility. *Nature Communications* **3** (2012).
2. Jean, J., Wang, A.N. & Bulovic, V. In situ vapor-deposited parylene substrates for ultra-thin, lightweight organic solar cells. *Organic Electronics* **31**, 120-126 (2016).
3. Yao, H.F. et al. Design and Synthesis of a Low Bandgap Small Molecule Acceptor for Efficient Polymer Solar Cells. *Advanced Materials* **28**, 8283-8287 (2016).
4. Song, X. et al. Controlling Blend Morphology for Ultrahigh Current Density in Nonfullerene Acceptor-Based Organic Solar Cells. *Acs Energy Lett* **3**, 669-676 (2018).
5. Wang, R. et al. High efficiency non-fullerene organic solar cells without electron transporting layers enabled by Lewis base anion doping. *Nano Energy* **51**, 736-744 (2018).
6. Chen, J.D. et al. Single-Junction Polymer Solar Cells Exceeding 10% Power Conversion Efficiency. *Advanced Materials* **27**, 1035-1041 (2015).
7. He, Z.C. et al. Single-junction polymer solar cells with high efficiency and photovoltage. *Nature Photonics* **9**, 174-179 (2015).
8. Liao, S.H., Jhuo, H.J., Cheng, Y.S. & Chen, S.A. Fullerene Derivative-Doped Zinc Oxide Nanofilm as the Cathode of Inverted Polymer Solar Cells with Low-Bandgap Polymer (PTB7-Th) for High Performance. *Advanced Materials* **25**, 4766-4771 (2013).
9. Cheng, P. et al. Alloy Acceptor: Superior Alternative to PCBM toward Efficient and Stable Organic Solar Cells. *Advanced Materials* **28**, 8021-8028 (2016).
10. Seo, K.W., Lee, J.H., Kim, H.J., Kim, H.K. & Na, S.I. Highly transparent and flexible InTiO/Ag nanowire/InTiO films for flexible organic solar cells. *Applied Physics Letters* **105** (2014).
11. Hecht, D.S., Hu, L.B. & Irvin, G. Emerging Transparent Electrodes Based on Thin Films of Carbon Nanotubes, Graphene, and Metallic Nanostructures. *Advanced Materials* **23**, 1482-1513 (2011).
12. Eda, G., Fanchini, G. & Chhowalla, M. Large-area ultrathin films of reduced graphene oxide as a transparent and flexible electronic material. *Nature Nanotechnology* **3**, 270-274 (2008).
13. Lee, J.Y., Connor, S.T., Cui, Y. & Peumans, P. Solution-processed metal nanowire mesh transparent electrodes. *Nano Letters* **8**, 689-692 (2008).
14. Seo, K.W. et al. Simple brush painted Ag nanowire network on graphene sheets for flexible organic solar cells. *Journal of Vacuum Science & Technology A* **32** (2014).
15. Ahn, J. et al. Extremely Robust and Patternable Electrodes for Copy-Paper-Based Electronics. *ACS Applied Materials & Interfaces* **8**, 19031-19037 (2016).
16. Im, H.G. et al. Hybrid crystalline-ITO/metal nanowire mesh transparent electrodes and their application for highly flexible perovskite solar cells. *Npg Asia Materials* **8** (2016).
17. Seo, J.W. et al. Facilitated embedding of silver nanowires into conformally-coated iCVD polymer films deposited on cloth for robust wearable electronics. *Nanoscale* **9**, 3399-3407 (2017).
18. Yu, Z.B., Li, L., Zhang, Q.W., Hu, W.L. & Pei, Q.B. Silver Nanowire-Polymer Composite Electrodes for Efficient Polymer Solar Cells. *Advanced Materials* **23**, 4453-+ (2011).
19. Song, M. et al. Highly Efficient and Bendable Organic Solar Cells with Solution-Processed Silver Nanowire Electrodes. *Advanced Functional Materials* **23**, 4177-4184 (2013).
20. Hu, L.B., Kim, H.S., Lee, J.Y., Peumans, P. & Cui, Y. Scalable Coating and Properties of Transparent, Flexible, Silver Nanowire Electrodes. *Acs Nano* **4**, 2955-2963 (2010).
21. Tokuno, T. et al. Fabrication of silver nanowire transparent electrodes at room temperature. *Nano Research* **4**, 1215-1222 (2011).
22. Lee, J., Lee, I., Kim, T.S. & Lee, J.Y. Efficient Welding of Silver Nanowire Networks without Post-Processing. *Small* **9**, 2887-2894 (2013).
23. Jin, J. et al. High-performance hybrid plastic films: a robust electrode platform for thin-film optoelectronics. *Energy Environ. Sci.* **6**, 1811-1817 (2013).
24. Li, D., Ouyang, G., McCann, J.T. & Xia, Y.N. Collecting electrospun nanofibers with

patterned electrodes. *Nano Letters* **5**, 913-916 (2005).
25. Jo, H.S. et al. Highly flexible, stretchable, patternable, transparent copper fiber heater on a complex 3D surface. *Npg Asia Materials* **9** (2017).
26. Choi, Y.-I. et al. Stretchable and transparent nanofiber-networked electrodes based on nanocomposites of polyurethane/reduced graphene oxide/silver nanoparticles with high dispersion and fused junctions. *Nanoscale* **11**, 3916-3924 (2019).
27. Azuma, K. et al. Facile fabrication of transparent and conductive nanowire networks by wet chemical etching with an electrospun nanofiber mask template. *Materials Letters* **115**, 187-189 (2014).
28. Bao, C.X. et al. In Situ Fabrication of Highly Conductive Metal Nanowire Networks with High Transmittance from Deep-Ultraviolet to Near-Infrared. *Acs Nano* **9**, 2502-2509 (2015).
29. Jorgensen, M., Norrman, K. & Krebs, F.C. Stability/degradation of polymer solar cells. *Solar Energy Materials and Solar Cells* **92**, 686-714 (2008).
30. Tsai, T.C., Chang, H.C., Chen, C.H., Huang, Y.C. & Whang, W.T. A facile dedoping approach for effectively tuning thermoelectricity and acidity of PEDOT:PSS films. *Organic Electronics* **15**, 641-645 (2014).
31. Sun, Y.M., Seo, J.H., Takacs, C.J., Seifter, J. & Heeger, A.J. Inverted Polymer Solar Cells Integrated with a Low-Temperature-Annealed Sol-Gel-Derived ZnO Film as an Electron Transport Layer. *Advanced Materials* **23**, 1679-+ (2011).
32. de Jong, M.P., van Ijzendoorn, L.J. & de Voigt, M.J.A. Stability of the interface between indium-tin-oxide and poly(3,4-ethylenedioxythiophene)/poly(styrenesulfonate) in polymer light-emitting diodes. *Applied Physics Letters* **77**, 2255-2257 (2000).
33. Choi, J. et al. Junction-Free Electrospun Ag Fiber Electrodes for Flexible Organic Light-Emitting Diodes. *Small* **14** (2018).
34. Lei, T. et al. Bendable and foldable flexible organic solar cells based on Ag nanowire films with 10.30% efficiency. *Journal of Materials Chemistry A* **7**, 3737-3744 (2019).
35. De, S. et al. Silver Nanowire Networks as Flexible, Transparent, Conducting Films: Extremely High DC to Optical Conductivity Ratios. *Acs Nano* **3**, 1767-1774 (2009).
36. Wu, H. et al. A transparent electrode based on a metal nanotrough network. *Nature Nanotechnology* **8**, 421-425 (2013).
37. Na, S.I., Kim, S.S., Jo, J. & Kim, D.Y. Efficient and Flexible ITO-Free Organic Solar Cells Using Highly Conductive Polymer Anodes. *Advanced Materials* **20**, 4061-4067 (2008).
38. Yu, Z.B. et al. Highly Flexible Silver Nanowire Electrodes for Shape-Memory Polymer Light-Emitting Diodes. *Advanced Materials* **23**, 664-+ (2011).
39. Kim, A., Won, Y., Woo, K., Kim, C.H. & Moon, J. Highly Transparent Low Resistance ZnO/Ag Nanowire/ZnO Composite Electrode for Thin Film Solar Cells. *Acs Nano* **7**, 1081-1091 (2013).
40. Gaynor, W., Burkhard, G.F., McGehee, M.D. & Peumans, P. Smooth Nanowire/Polymer Composite Transparent Electrodes. *Advanced Materials* **23**, 2905-2910 (2011).
41. Choi, D.Y., Kang, H.W., Sung, H.J. & Kim, S.S. Annealing-free, flexible silver nanowire-polymer composite electrodes via a continuous two-step spray-coating method. *Nanoscale* **5**, 977-983 (2013).
42. O'Connor, T.F. et al. Wearable organic solar cells with high cyclic bending stability: Materials selection criteria. *Solar Energy Materials and Solar Cells* **144**, 438-444 (2016).
43. Sun, Y.G., Yin, Y.D., Mayers, B.T., Herricks, T. & Xia, Y.N. Uniform silver nanowires synthesis by reducing AgNO3 with ethylene glycol in the presence of seeds and poly(vinyl pyrrolidone). *Chemistry of Materials* **14**, 4736-4745 (2002).
44. Yang, C. et al. Silver Nanowires: From Scalable Synthesis to Recyclable Foldable Electronics. *Advanced Materials* **23**, 3052-+ (2011).
45. Sun, Y.G., Mayers, B., Herricks, T. & Xia, Y.N. Polyol synthesis of uniform silver nanowires: A plausible growth mechanism and the supporting evidence. *Nano Letters* **3**, 955-960 (2003).
46. Park, S.D. et al. Etch characteristics of silver by inductively coupled fluorine-based plasmas. *Thin Solid Films* **445**, 138-143 (2003).

47. Park, S.D. et al. Influence of substrate temperature on the etching of silver films using inductively coupled Cl-2-based plasmas. *Surface & Coatings Technology* **171**, 285-289 (2003).
48. Cha, H.C. et al. Performance improvement of large-area roll-to-roll slot-die-coated inverted polymer solar cell by tailoring electron transport layer. *Solar Energy Materials and Solar Cells* **130**, 191-198 (2014).

Acknowledgments

This work was supported by the National Research Foundation of Korea (NRF) grant funded by the Korea government (MSIT) (No. NRF-2019R1A2C3008035 and NRF-2015M1A2A2057509).

Author contributions

K.-W. S, J.L., and J. J contributed equally to this work. K.-W. S., J.L., J. J., and J.-Y. L conceived and designed the experiments and prepared the manuscript; K.-W. S. and J. L. fabricated all the transparent electrodes used in this study and analyzed the results; J. J. fabricated and characterized flexible organic solar cells; C. C. performed optical, electrical simulations and analyzed the results. All authors discussed the results and commented on the manuscript.

Additional information

Competing financial interests: the authors declare no competing financial interests.

Figure Legends

Figure 1 | Formation of zero-junction Ag NN electrode. (**a**) Schematic illustration for the fabrication of monolithic, etched NNs using nanofiber networks as a mask. **I,** Deposition of a thin metal film on a substrate. **II,** Coating electrospun nanofibers on the metal film to form a nanomask. **III,** Etching the metal film. **IV,** Removing residue to complete the fabrication of the NN. (**b**) The electrospun nanofibers on thin Ag films (**c**). The etched NNs formed using electrospun nanofibers as a nanomask. The inset shows the trapezoidal edge of an etched network. AFM images of (**d**) an ordinary AgNW network and (**e**) an etched NN with a uniform height distribution and seamless junctions.

Figure 2 | High quality of Ag NN electrode. (**a**) Optoelectrical characteristics comparison of several transparent electrodes and AgNN electrodes. AgNN electrode sheet resistance and optical transmittance with (**b**) various density, thickness, and (**c**) formed on various substrates. (**d**) Resistance change of ITO, AgNWs, AgNN electrodes with decreasing bending radius (top) and increasing bending cycles (bottom).

Figure 3 | Fabrication FOSCs using Ag NN electrode. (**a**) Schematic illustration of an inverted FOSCs and energy levels of active layers using PTB7-Th donor and $PC_{70}BM$ and IEICO-4F acceptors. (**b**) *J-V* characteristics and (**c**) EQE spectra of ITO and AgNN electrode devices using both fullerene and non-fullerene acceptors. (**d**) Maximum obtained PCE and device yield with initial Ag film thickness. (**e**) PCE of non-fullerene acceptor based FOSCs with different NN coverages. η_G: charge generation, η_C: charge collection efficiencies.

Figure 4 | Bending test results of FOSCs. (**a**) Photographs of bending test. (**b**) PCE degradation of fullerene acceptor based FOSCs using ITO and AgNN electrodes with increasing bending cycles. *J-V* characteristics change of (**c**) ITO, and (**d**), AgNN electrode based FOSCs.

Tables

Table 1 | The photovoltaic performance of FOSCs fabricated on ITO and AgNN electrodes

	PTB7-Th:$PC_{70}BM$		PTB7-Th:IEICO-4F	
Performance	**ITO**	**AgNN**	**ITO**	**AgNN**
PCE [%]	8.35	8.31	9.59	10.6
J_{sc} [mA/cm^2]	15.7	15.01	23.3	24.3
V_{oc} [V]	0.79	0.79	0.67	0.69
FF	0.68	0.70	0.61	0.63

Table of contents entry

The PEDOT-free and ITO-free junction-free AgNN electrode with high optoelectrical properties is proposed for FOSCs. The electrical sheet resistance and optical transmittance could be controlled by both initial metal thickness and NN density; even very thin Ag layer with appropriate NN density can show high transmittance and low sheet resistance, yielding highly efficient FOSC.

Keywords:
PEDOT-free, ITO-free, AgNN, transparent electrodes, flexible organic solar cells

Ki-Won Seo, Jaemin Lee, Jiwhan Jo, Changsoon Cho, and Jung-Yong Lee

Highly efficient (>10%) flexible organic solar cells on PEDOT and ITO-free transparent electrodes

ToC figure